Journal of proteome research

pubs.acs.org/jpr

Article

Deep Proteome of the Developing Chick Midbrain

Kaitlyn E. Stepler, Seth C. Hannah, Lisa A. Taneyhill,* and Peter Nemes*

Cite This: *J. Proteome Res.* 2023, 22, 3264−3274

Read Online

ACCESS | Metrics & More | Article Recommendations | Supporting Information

ABSTRACT: The epithelial-to-mesenchymal transition (EMT) and migration of cranial neural crest cells within the midbrain are critical processes that permit proper craniofacial patterning in the early embryo. Disruptions in these processes not only impair development but also lead to various diseases, underscoring the need for their detailed understanding at the molecular level. The chick embryo has served historically as an excellent model for human embryonic development, including cranial neural crest cell EMT and migration. While these developmental events have been characterized transcriptionally, studies at the protein level have not been undertaken to date. Here, we applied mass spectrometry (MS)-based proteomics to establish a deep proteomics profile of the chick midbrain region during early embryonic development. Our proteomics method combines optimal lysis conditions, offline fractionation, separation on a nanopatterned stationary phase (μPAC) using nanoflow liquid chromatography, and detection using quadrupole−ion trap−Orbitrap tribrid high-resolution tandem MS. Identification of >5900 proteins and >450 phosphoproteins in this study marks the deepest coverage of the chick midbrain proteome to date. These proteins have known roles in pathways related to neural crest cell EMT and migration such as signaling, proteolysis/extracellular matrix remodeling, and transcriptional regulation. This study offers valuable insight into important developmental processes occurring in the midbrain region and demonstrates the utility of proteomics for characterization of tissue microenvironments during chick embryogenesis.

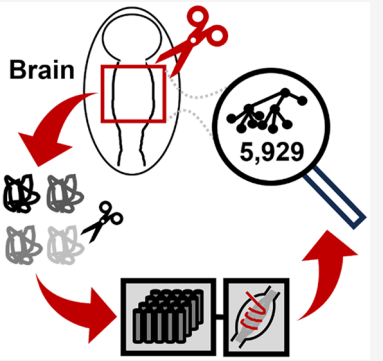

KEYWORDS: *chick embryo, epithelial-to-mesenchymal transition (EMT), mass spectrometry, cranial neural crest, proteomics*

INTRODUCTION

An important key in understanding human development and disease is access to and use of an appropriate animal model, such that results will be directly translatable. The chick embryo fits these criteria due to its large size, external development, and ease of experimental manipulation. During neurulation of the developing chick embryo, cranial neural crest cells in the dorsal neural tube of the midbrain undergo an epithelial-to-mesenchymal transition (EMT), delaminate, and migrate through the mesenchyme, where they differentiate into neurons, glia, chondrocytes, and osteocytes. In humans, disruptions in this process can result in developmental disorders affecting the craniofacial structure and peripheral nervous system function, and the molecular mechanisms underlying EMT and migration are shared with cancer metastasis. Studies utilizing single-cell RNA sequencing of migrating cranial neural crest cells in developing chick embryos have been conducted to identify key molecular factors.[1] While gene-by-gene screening of transcripts has uncovered key molecular regulators of the developing midbrain region, defined herein to include the neural tube, ectoderm, cranial neural crest cells, and cranial mesenchyme, direct identification of the proteomic profile of this region has been elusive.

Due to the complex relationship between transcription, translation, and posttranslational modifications (PTMs), especially in developing systems,[2,3] validation of gene expression is essential at the level of the proteome. Methods using antibody-based detection, such as Western blots and enzyme-linked immunosorbent assays (ELISAs), have long provided a lifeline for validating protein expression. These approaches, however, require known protein targets and functional antibodies and operate only one gene at a time at best, thus limiting these studies to single or few proteins.[4,5] While these methods remain valuable for measuring targeted proteins with high sensitivity, mass spectrometry (MS)-based proteomics has become the gold standard for both untargeted and targeted proteomics. High-resolution MS (HRMS) technology allows for obtaining sequence information and accurate quantification of thousands of proteins from a single sample,[6,7] furthering the validation of antibody-based assays such as the Western blot in animals[5,8] and plants[9] alike.

MS-based proteomics has emerged as a tool to study a range of developmental processes. The chick embryo has supported studies on facial development,[10] retinogenesis,[10] spatiotemporal development of the cardiovascular system,[11] sex differences,[12] and hepatic metabolism shifts during development.[13] The species has also aided protein expression studies in the

Received: May 13, 2023
Published: August 24, 2023

https://doi.org/10.1021/acs.jproteome.3c00291
J. Proteome Res. 2023, 22, 3264−3274

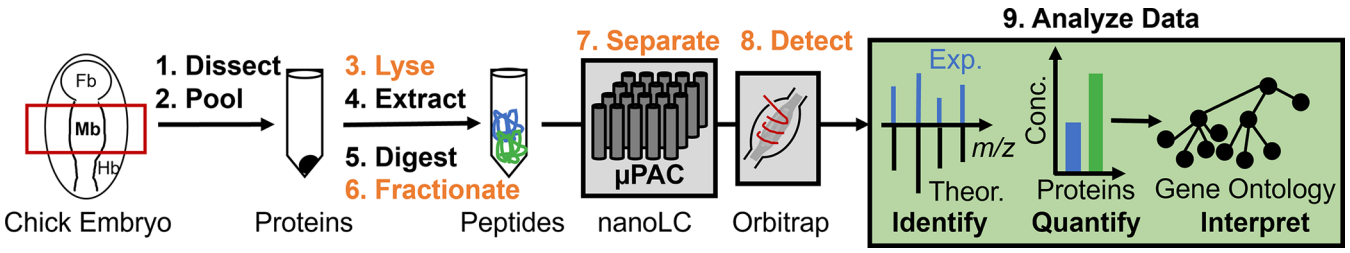

Figure 1. Experimental strategy to enable deep proteomic characterization of the chick embryonic midbrain using high-resolution mass spectrometry (HRMS). The midbrains (Mb) were dissected, pooled, processed using a bottom-up proteomics workflow, and measured by micropillar array column (μPAC) nanoflow liquid chromatography (nanoLC) and HRMS. Steps highlighted in orange were systematically assessed in this study. The qualitative and quantitative information resulting from these analyses supported gene regulatory pathway analyses of early developmental processes. Key: Fb, forebrain; Hb, hindbrain.

context of a neural crest-derived cell line.[14] However, while transcriptomics has characterized the expression of 14,536 genes at embryonic day (E)1 in whole chick embryos,[15] deep HRMS-based proteomics has not been used to assess early embryonic development, with the earliest existing study starting at E3.[16] Moreover, most proteomics studies in the chick embryo have utilized one- or two-dimensional gel electrophoresis separation in combination with downstream MS analysis, detecting up to ∼1500 proteins,[10] though some data sets were limited to only tens[17] to hundreds[16] of proteins. In contrast, using solution-based sample preparation followed by hyphenated nanoflow liquid chromatography (nanoLC)−HRMS analysis, 2195 protein groups (2926 unique proteins) have been identified from whole brain at E18,[12] showcasing the significant improvement in proteome coverage that can be achieved. Contemporary LC stationary phases[18] and HRMS instrumentation[12,19] offer valuable resources to further deepen these analyses, yet remain untapped for studying the brain in the chick embryo, particularly during early embryonic development.

In this study, our goal was to leverage recent developments in nanoLC-HRMS to characterize the deep proteome of the developing midbrain region of the early chick embryo. We aimed to investigate the midbrain at 6−8 somite stages of development (<E1.5), when EMT and migration of cranial neural crest cells occur as a first step in embryonic patterning. We proposed to deepen proteome coverage from limited tissues by systematically revising and refining main steps of the bottom-up proteomics workflow, specifically cell lysis, offline fractionation, and nanoLC-HRMS (Figure 1). This study provided the first proteomic profile of this region in the developing chick embryo to date, achieving record coverage of >5900 proteins. Gene ontology annotation of the proteins returned important biological pathways for early development, ranging from signaling to proteolysis/extracellular matrix remodeling, to transcriptional regulation. This data set offers valuable insight into essential developmental processes in the chick embryonic midbrain. The HRMS-based proteomics approaches developed here can be adapted to characterize other tissues during early chick embryogenesis.

MATERIALS AND METHODS

Chemicals

Nonidet P-40 (NP-40, 10% w/v) substitute and complete mini ethylenediaminetetraacetic acid (EDTA)-free protease inhibitor tablets were obtained from Roche (Basel, Switzerland). Dithiothreitol (DTT) and iodoacetamide (IAA) were purchased from Sigma-Aldrich (St. Louis, MO, USA). Sodium dodecyl sulfate (SDS) and glycerol were purchased from Amresco (Solon, OH, USA). Ammonium bicarbonate was obtained from J. T. Baker (Phillipsburg, NJ, USA). NaCl was obtained from Macron Fine Chemicals (Allentown, PA, USA). Tris-HCl (1 M), EDTA (0.5 M), acetone, and $CaCl_2$ were supplied by Fisher Scientific (Pittsburgh, PA, USA). For the instrumental proteomics workflow, Pierce trypsin protease (MS-grade) and LC-MS-grade acetonitrile (ACN), water, and formic acid (FA) were purchased from Fisher Scientific (Pittsburgh, PA, USA).

Solutions

Ringer's solution (containing 125 mM NaCl, 1.5 mM $CaCl_2$, 5 mM KCl, 0.8 mM Na_2HPO_4, and 1.5 mM KH_2PO_4), lysis buffer (containing 1% w/v SDS, 150 mM NaCl, 5 mM EDTA, 20 mM Tris-HCl), modified lysis buffer (containing 25 mM Tris-HCl adjusted to pH 7.4, 150 mM NaCl, 1 mM EDTA, 1% (w/v) NP-40 substitute, and 5% (v/v) glycerol, supplemented with 1 mM $CaCl_2$ and a protease inhibitor tablet), and proteome digestion buffer (containing 50 mM ammonium bicarbonate adjusted to pH 8 with Tris) were used.

Isolation of the Chick Midbrain

Fertilized chicken eggs (*Gallus gallus*) were acquired from the University of Maryland (College Park, MD, USA) and incubated for 33 h at 38 °C in a humidified incubator. Using an 18-gauge needle and syringe, 5 mL of the egg albumen was removed to allow a small viewing window to be cut out of the shell. Using a 27-gauge needle and syringe, Ringer's solution containing India ink was injected under the embryo to provide visual contrast (Figure 2A). The embryos were imaged under a stereomicroscope and staged based on the number of somite pairs (6−8 somite pairs, Figure 2B)[20] before being removed from the egg and placed in a Petri dish containing Ringer's solution (Figure 2C). The midbrain was microdissected using tungsten needles, as published elsewhere.[21] For each sample, 27−30 midbrains were pooled and centrifuged at 500*g* for 5 min. The supernatant was removed, and the pellet was flash frozen in liquid nitrogen and stored at −80 °C until measurement.

Proteomics Analysis

The dissected midbrain tissues were dissolved in 75 μL of proteome lysis buffer and agitated by gentle pipetting to facilitate cell lysis and protein extraction. The resulting lysate was centrifuged at 20817*g* (max speed) at 4 °C to remove cell debris. For sample preparation using a modified lysis buffer, the tissues were dissolved and pipetted as above, followed by lysis for 30 min at 4 °C with rocking and occasional

https://doi.org/10.1021/acs.jproteome.3c00291
J. Proteome Res. 2023, 22, 3264−3274

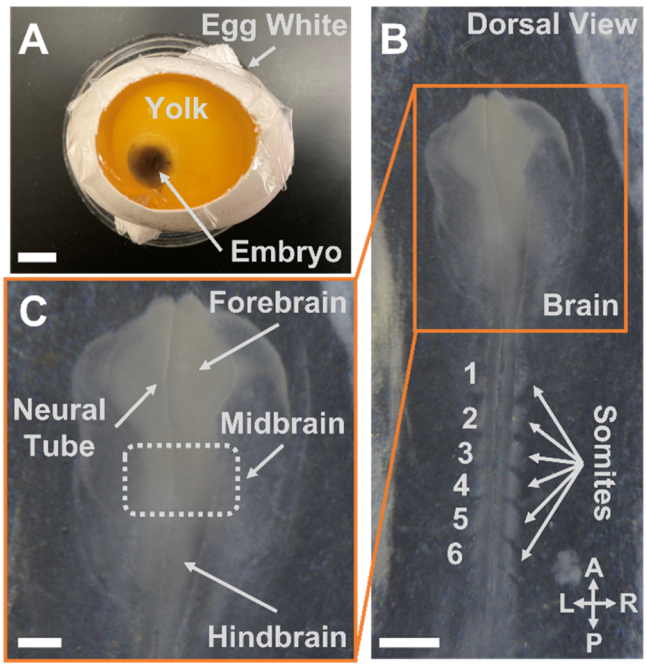

Figure 2. Microdissection of the midbrain from chick embryos. (A) A hemidissected egg showing the embryo against a co-injected contrast dye. (B) Dorsal view of an excised embryo at Hamburger–Hamilton stage 9, highlighting key anatomical regions. Key to axes: A(nterior); L(eft); P(osterior); R(ight). (C) Close-up image of the embryo highlighting the dissected midbrain region. Scale bars: 10 mm (panel A), 0.5 mm (panel B), and 0.1 mm (panel C).

vortexing.[21] The lysate was then spiked with 10% (w/v) SDS for a final concentration of 0.1% SDS to denature proteins.

The proteins were processed via a typical bottom-up workflow. The protein disulfide bonds were reduced (3 μL of 0.5 M DTT, 60 °C, 30 min) and alkylated (9 μL of 0.5 M IAA, 20 min, dark, room temperature). Alkylation was quenched using the same DTT treatment, with vortexing. The extracted proteins were precipitated overnight at −20 °C with chilled acetone, pelleted via centrifugation at 10000*g* at 4 °C for 10 min, and reconstituted in the proteome digestion buffer after supernatant removal. From each sample, ∼100 μg of protein was digested (1:50 trypsin:protein ratio, 37 °C, 12 h). The peptides were vacuum-dried (CentriVap, Labconco, Kansas City, MO, USA), desalted (Pierce peptide desalting spin columns, Thermo), and quantified to estimate the total amount (Take 3, Agilent Technologies, Santa Clara, CA, USA). Unfractionated samples were reconstituted to 0.5 μg/μL in 0.1% (v/v) FA for LC-HRMS analysis. For experiments using fractionation, the desalted peptide sample was fractionated at high pH (Pierce high-pH reversed-phase peptide fractionation kit, Thermo) using a gradient of ACN at 7.5%, 15%, 22.5%, 30%, 50%, and 80% (v/v) containing 0.1% (v/v) triethylamine. The resulting six fractions were each reconstituted in 0.1% FA for nanoLC-HRMS analysis (above).

The samples and fractions were measured in technical duplicate (0.5 μg each) on an UltiMate 3000 RSLCnano system (Thermo) coupled to an Orbitrap Fusion Lumos mass spectrometer (Thermo). Mobile phase A was 0.1% FA in water, and mobile phase B was 0.1% FA in ACN. Peptides were trapped in 100% A at 5.0 μL/min on an Acclaim PepMap 100 C_{18} column (Thermo, 100 μm × 2 cm, 100 Å, 5 μm) and separated on a micropillar array column (μPAC, Thermo; 200 cm, 50 °C) at 600 nL/min over a 240 min gradient as follows: 0–5 min, 1% B; 5–20 min, 1–7% B; 20–135 min, 7–25% B; 135–160 min, 25–32% B; 160–193 min, 32–45% B; 193–200 min, 45–75% B; 200–208 min, 75% B; 208–210 min, 75–2% B; 210–240 min, 2% B. Full MS spectra were collected in the positive ion mode in the Orbitrap analyzer using the following settings: m/z 350–1500, 120,000 full width at half-maximum (fwhm) resolution, standard automatic gain control (AGC) target, 50 ms maximum injection time. MS/MS scans were collected in the ion trap with a data-dependent acquisition (DDA) mode executing a 3 s cycle time and higher-energy collisional dissociation (HCD) using the following conditions: 30% normalized collision energy, auto scan range mode, 1.6 m/z isolation window, rapid ion trap scan rate, standard AGC target, dynamic maximum injection time mode, and dynamic exclusion of the fragmented ions for 60 s. The peptide monoisotopic peak determination node was enabled, and precursor ions were required to have charges between +2 and +7 and intensity >5.0 × 10^3 counts for consideration for MS/MS.

Alternatively, measurements utilized data-independent acquisition (DIA) analyses. The same nanoLC gradient and parameters were used with DIA as earlier. Survey MS spectra were recorded as with the DDA analyses, except the auto maximum injection time mode was used and advanced peak determination was turned on. Tandem MS spectra were acquired in DIA mode in the Orbitrap using HCD (30% normalized collision energy, 30,000 fwhm resolution, auto scan range mode, 12 m/z windows, 1 m/z window overlap, standard AGC target, auto maximum injection time mode) with window placement optimization enabled.

Data Analysis

Proteomics. The primary DDA MS-MS/MS files were analyzed in Proteome Discoverer version 2.2. For the fractionated samples, all fractions and technical replicates were combined to produce a single result file. Each file was searched against the UniProt *Gallus gallus* reviewed and unreviewed proteome (27,535 sequences, downloaded on 3/25/2022), as well as a database of common contaminants, using SEQUEST-HT. Dynamic modifications included in each search were oxidation of methionine residues and acetylation of the protein N-termini. Although the experiments were not design to implement phosphopeptide enrichment, we searched the proteomics data for optional phosphorylation at serime/threonine residues. Carbamidomethylation on cysteine residues was included as a fixed modification in all searches. The search allowed two trypsin missed cleavages and used mass tolerances of 10 ppm for precursor ions and 0.6 Da for fragment ions. Only peptides and proteins with a false discovery rate (FDR) of <1%, calculated against a reversed-sequence decoy database, were included in the final report. Common contaminant proteins were manually curated and excluded from proteins identified in this study. Proteins were required to have ≥1 unique peptide for identification and quantification. Concentrations were assessed using label-free quantification (LFQ). Precursor LFQ intensities were normalized to total peptide signal abundance.

DIA data files were analyzed using DIA-NN version 1.8.1[22] with a library-free search against the same UniProt database. The same modifications were included in the search, with the addition of N-terminal methionine excision and a maximum of three variable modifications. Two trypsin miscleavages were

https://doi.org/10.1021/acs.jproteome.3c00291
J. Proteome Res. 2023, 22, 3264−3274

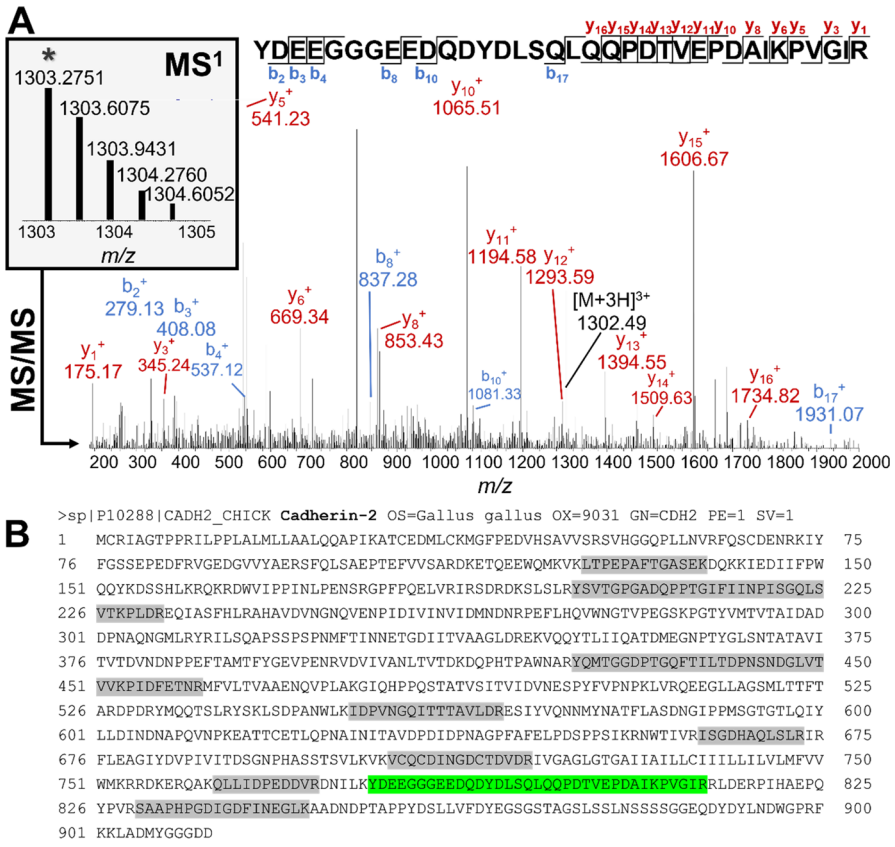

Figure 3. HRMS identification of a representative protein. (A) Survey (MS^1) scans detected the presence of an ion with m/z 1303.2751, triggering MS/MS sequencing that identified a proteotypic peptide for cadherin-2 (UniProt accession number P10288). Annotated *b* (blue) and *y* (red) ions are labeled on the MS/MS spectrum. (B) Example of identifying the cadherin-2 protein based on the sequencing of a total of nine different proteotypic peptides (highlighted in gray), providing ∼20% coverage of the total protein sequence.

allowed. Peptide length range was set to 6−144 amino acids (same as the DDA search). Precursor and fragment ions were detected between m/z 350 and 1500. Technical replicates were searched together using the match-between-runs algorithm. Protein inference was set to "Protein Names (from FASTA)". Quantification mode was set to "Robust LC (high precision)". Precursors were filtered to FDR < 1%. All other parameters were set to the default settings. Identifications reported to contain multiple entries in the group name were removed from this report to produce the final list of unique identified proteins.

Gene Ontology and Pathway Analysis. Gene Ontology and Reactome[23] pathway annotation was performed using the PANTHER database version 17.0[24] (released on February 22, 2022). STRING version 11.5[25] was used to map protein−protein interactions for pathways of interest (with a minimum required interaction score of 0.400 for medium confidence).

Safety

Biological samples and chemicals were handled with care utilizing appropriate personal protective equipment and following standard safety protocols.

Data Repository

The MS proteomics data have been deposited to the ProteomeXchange Consortium (http://proteomecentral.proteomexchange.org) via the PRIDE partner repository[26] with the data set identifier PXD042200.

RESULTS AND DISCUSSION

Rationale for the Study

The developing midbrain of the chick embryo (defined herein to include the neural tube, ectoderm, cranial neural crest cells, and cranial mesenchyme) is a powerful biological model for multiple complex biological processes including the EMT and migration of cranial neural crest cells. These cells migrate throughout the cranial mesenchyme and eventually differentiate into diverse derivatives, including chondrocytes and osteocytes, to generate craniofacial structures, pigment-containing melanocytes, neurons of the autonomic and sensory ganglia of the peripheral nervous system, and their supporting glial cells.[27] Identifying the proteins that regulate these processes in the chick midbrain would facilitate the understanding of development and disease. However, manual dexterity required for microdissection of the tissue from a live, developing system and availability of limited amounts of proteins for analysis (∼0.5−2 μg protein per midbrain) have so far hindered the sensitivity of HRMS-based proteomics in the chick midbrain, particularly for low-abundance proteins of significance to early development. To remedy these challenges, we aimed to develop a HRMS-based proteomics approach with deepened coverage of the proteome in the early developing midbrain of the chick.

Proteomics Method Development

We initially tested a typical bottom-up proteomics approach for the embryonic midbrain, as shown in Figure 1. The midbrain region, shown in Figure 2, was dissected and pooled

https://doi.org/10.1021/acs.jproteome.3c00291
J. Proteome Res. 2023, 22, 3264−3274

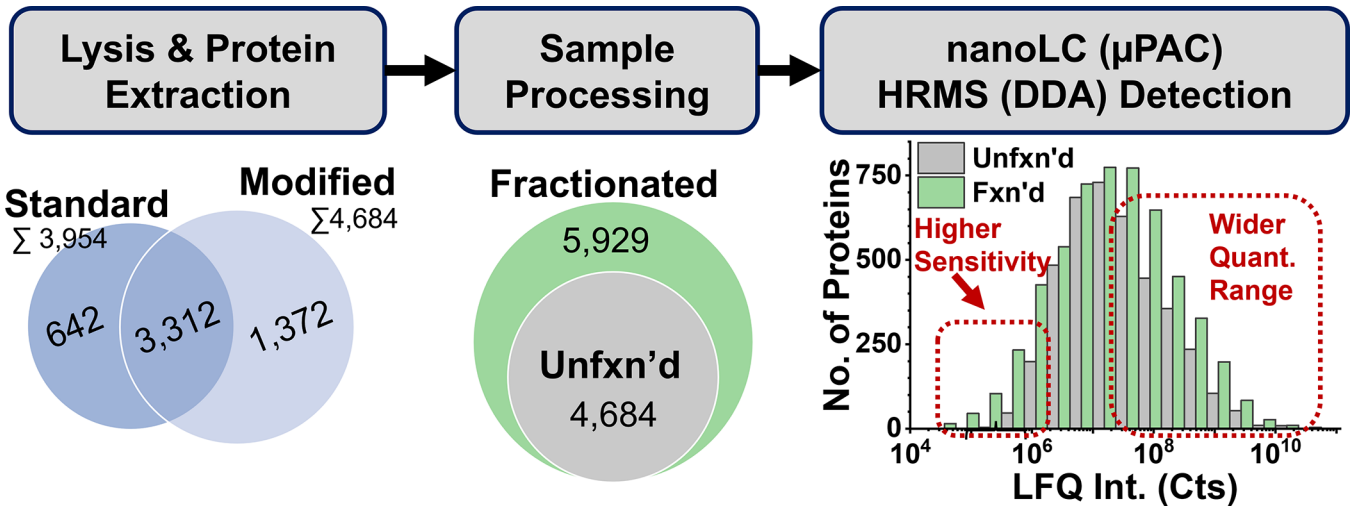

Figure 4. Enhancement of detection sensitivity through the systematic refinement of sample processing. The workflow steps of tissue lysis and protein extraction (lysis buffer composition) and bottom-up proteomics sample preparation (addition of offline fractionation, Fxn) were evaluated using a new-generation micropillar array column (μPAC) for nanoLC and HRMS executing data-dependent acquisition (DDA). Label-free quantification (LFQ) with median scaling of the calculated protein intensities revealed comparable sensitivity for the majority of the 3993 proteins quantified without sample fractionation (Unfxn'd) and the 5383 proteins measured through 6-plexed high-pH fractionation (Fxn'd). Fractionation expanded the linear dynamic range of quantification at both extremes, notably improving sensitivity for low-abundance proteins.

from 27−30 embryos at the 6−8 somite stage, representing the early phase of cranial neural crest cell EMT and migration. Pooled tissues were then lysed, and the extracted proteome was processed using a typical bottom-up proteomics approach, in which cysteine residues on proteins were reduced and alkylated. The proteome was purified by cold acetone overnight precipitation and digested into peptides using trypsin. The resulting peptide mixture was desalted prior to the nanoLC-HRMS measurement of 0.5 μg of peptides. This loading amount was selected to maximize proteome coverage, reduce sample consumption for technical replicates, and extend column lifetime. We utilized a new-generation μPAC for reversed-phase nanoLC separation, as it has recently been shown to improve separation efficiency and reproducibility[18] and improve protein/peptide identifications.[28] During subsequent HRMS identification of peptides and proteins, the MS/MS spectra were matched to the theoretical fragmentation spectra. These data provided both qualitative and quantitative information about the proteomes, supporting gene ontology annotation of canonical molecular roles and functions.

With this standard shotgun proteomics workflow, 3954 total proteins were identified from ∼30 pooled midbrains. Figure 3 presents an example where the cadherin-2 protein was identified at ∼20% sequence coverage based on the sequencing of nine different proteotypic peptides. The detected proteins are listed in Table S1. This detected proteome marks the first discovery characterization of the midbrain in early-stage developing chick embryos. Although proteomics has previously been adapted to the brain (whole brain[12] and specific regions[29,30]), liver,[13] heart,[11] head tissues (i.e., branchial arch 1[16] and retina[10]), and cerebrospinal fluid[17] in the chick embryo, these studies targeted later stages of development (>E1.5) and yielded limited proteome coverage, identifying from ∼20−25[16,17] to ∼3400 proteins.[13] In comparison to earlier work in the brain using packed C_{18}-bed nanoLC with quadrupole−Orbitrap tandem HRMS,[12] our new-generation μPAC nanoLC with quadrupole−ion trap−Orbitrap tribrid tandem HRMS technology improved the number of identifiable proteins by ∼35%.

We proposed further sensitivity improvements by systematically refining major steps of the shotgun approach. As illustrated in Figure 4, we began with improving tissue lysis. $CaCl_2$ has been demonstrated to stabilize various Ca^{2+}-binding proteins in solution,[31,32] including several proteins involved during cranial neural crest cell EMT and migration, such as cadherins, calcineurin, and calcium-dependent kinases. Therefore, to facilitate the detection of these relevant proteins in this study, we supplemented the lysis buffer with $CaCl_2$ and protease inhibitors in combination with a 30 min lysis (vs instantaneous with pipet aspiration).[21] This modified lysis protocol increased overall proteome coverage to 4684 proteins (Figure 4). A list of measured proteins is available in Table S2. This modified approach also improved the confidence in protein identification for several Ca^{2+}-binding proteins of interest. For example, more peptide spectral matches (PSMs) were detected for cadherin-2, B-cadherin, and calcium/calmodulin-dependent protein kinase II delta (Table S1 vs S2). Furthermore, several additional members of the cadherin- and calcium/calmodulin-dependent protein kinase families became detectable compared to the standard method, demonstrating that the modified lysis improved both overall and Ca^{2+}-binding protein coverage.

Nesting a second dimension of separation prior to LC-MS analysis is also a well-established strategy to deepen proteome coverage, particularly using high-pH reversed-phase LC separation.[33−36] Therefore, we assessed this approach in our proteomics workflow for the chick midbrain using spin column-based fractionation. With six fractions, identifications improved by ∼26% to 5929 detected proteins (Figure 4, middle panel). The detected proteins are given in Table S3. The proportion of quantified proteins also increased to ∼90% compared to ∼85% in the unfractionated sample described above, including more low-abundance proteins (Figure 4). Comparison of the $\log_{10}$-transformed and median-normalized LFQ abundance indices revealed comparable concentrations

https://doi.org/10.1021/acs.jproteome.3c00291
J. Proteome Res. 2023, 22, 3264−3274

for the majority of the proteins between the approaches. Fractionation broadened the linear dynamic range of quantification by about an order of magnitude, improving quantitative sensitivity for lower-abundance proteins (Figure 4, right panel).

Last, we refined the method of HRMS data acquisition, which fundamentally controls the success of peptide sequencing and hence the fidelity of protein identifications. During DDA, historically the most commonly employed approach in bottom-up proteomics, the most abundant precursor ions are preferred for fragmentation, albeit at the expense of quantitative bias toward reporting on molecules at high concentration.[37,38] As an alternative, DIA schedules fragmentation for precursor ions over a wide m/z window, thus enhancing the likelihood of sequencing low-abundance peptides for trace-level protein identification.[39−43] The DIA data acquisition parameters were kept consistent with the DDA method when possible to facilitate a direct comparison of the results between the two methods. We selected 12 m/z windows for the DIA method based on recent publications using Orbitrap hybrid and tribrid instruments.[44,45] Surprisingly, DIA of the same midbrain proteome returned 4470 proteins (Table S4), slightly lower than the 4684 proteins (Table S2) that were detected by the DDA method on the same sample (Figure 5). All proteins (100%) identified by DIA

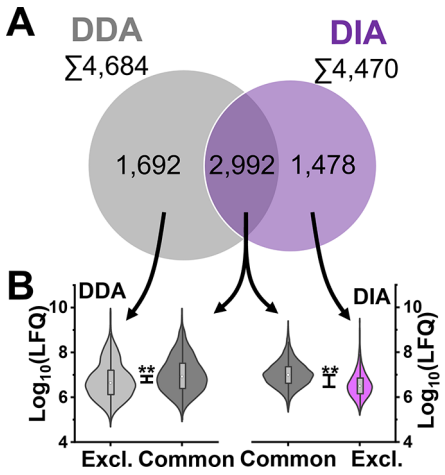

Figure 5. Impact of data acquisition on coverage of the detectable proteome. Comparison of (A) protein identification and (B) quantification from data-dependent acquisition (DDA) and data-independent acquisition (DIA) methods on the same midbrain proteome sample. A comparable number of proteins were identified using these methods with similar sensitivity.

were, however, reproducibly quantified among the technical replicates, while only ∼85% of all identified proteins were quantifiable across biological replicates by using DDA.

Closer inspection of the data revealed differences in the quantitative results. On average, ∼66% of proteins were commonly identified using DDA and DIA (2992 proteins, Figure 5A). A relatively large proportion of the detected proteome (approximately one-third) was exclusively identified using either DDA or DIA (1692 and 1478 proteins, respectively), revealing a rather complementary aspect of these two methods. As shown in Figure 5B, proteins that were exclusively quantifiable in DDA spread across the complete dynamic LFQ range, whereas those uniquely identifiable by DIA populated the lower domain of concentration, with these differences being statistically significant for both methods (DDA: $p = 4.7 \times 10^{-22}$; DIA: $p = 3.53 \times 10^{-134}$). Our findings in the chick midbrain proteome are in accordance with previous results on the quantitative performance of the methods in other biological systems,[38,42] further underscoring the complementary nature of the methods for protein quantification.

The identified proteome provides insights into the local tissue microenvironment. Our data were compared to canonical markers in the midbrain region, which includes the neural tube, ectoderm, cranial neural crest cells, and cranial mesenchyme. The midbrain-to-hindbrain boundary is defined by the most posterior expression of orthodenticle homeobox 2 (*Otx2*) and the most anterior expression of hindbrain gastrulation brain homeobox 2 (*Gbx2*).[46] Otx2 was identified in our data set without the detection of Gbx2. The transcription factor paired box gene 2 (Pax2) along with wingless/integrated (Wnt) family signaling proteins help maintain the midbrain-to-hindbrain boundary. *Pax2* is expressed in a gradient across the boundary, while wingless-type MMTV integration site family member 4 (*Wnt4*) is strongly expressed in the midbrain.[47] Consistent with these patterns, both Pax2 and Wnt4 were identified within our pooled sample, further validating the proteomic profile. Cadherins are integral to the EMT and are differentially expressed across the various tissues in this region. At these developmental stages, cadherin-1 is expressed in the ectoderm, cadherin-2 in the neural tube,[48] and cadherin-11 in migratory neural crest cells,[49] all of which were identified in our proteome.

Global Proteome Profile in the Developing Midbrain

The >5900 proteins that were measured in this study allow for the appreciation of molecular pathways underpinning embryonic patterning in previously inaccessible details. To date, the largest existing proteomics study of the embryonic chick brain has identified 2195 protein groups from whole brain at E18.[12] PANTHER[24] Gene Ontology annotation of proteins that were detected in our study represented several canonical pathways (Table S5). For the sake of brevity, Figure 6 presents 10 biological pathways with the most significant enrichment (Figure 6A). For nearly all, more proteins were identified using our improved method compared to our original method. For example, the number of proteins improved by 1.5-fold in the Wnt signaling pathway (92 vs 61 proteins, respectively) and the platelet-derived growth factor (PDGF) signaling pathway (52 vs 34 proteins), as shown in Figure 6B (see insets).

Given the important role of phosphorylation in neural crest cell EMT and migration, we also mined our data set for this PTM. Although our sample processing workflow was not designed to enrich for phosphorylated peptides or proteins in this study, >650 phosphorylated peptides corresponding to 454 proteins were detected in our data set (Table S6). Of the detected phosphorylation sites, the majority were on serine residues (542 peptides) with fewer on threonine (93 peptides) and tyrosine (24 peptides) residues. Notably, several known regulators involved in EMT were among these phosphorylated proteins, including β-catenin (CTNNB1), δ-catenin, or p120-catenin (CTNND1), Wnt1, Lin28B, and insulin-like growth factor 1 receptor (IGF1R). In what follows, we reflect on several pathways that are important for neural crest cell EMT and migration, specifically proteolysis/extracellular matrix remodeling, signaling pathways, and transcriptional regulation, highlighting the utility of our improved MS approach to help

https://doi.org/10.1021/acs.jproteome.3c00291
J. Proteome Res. 2023, 22, 3264−3274

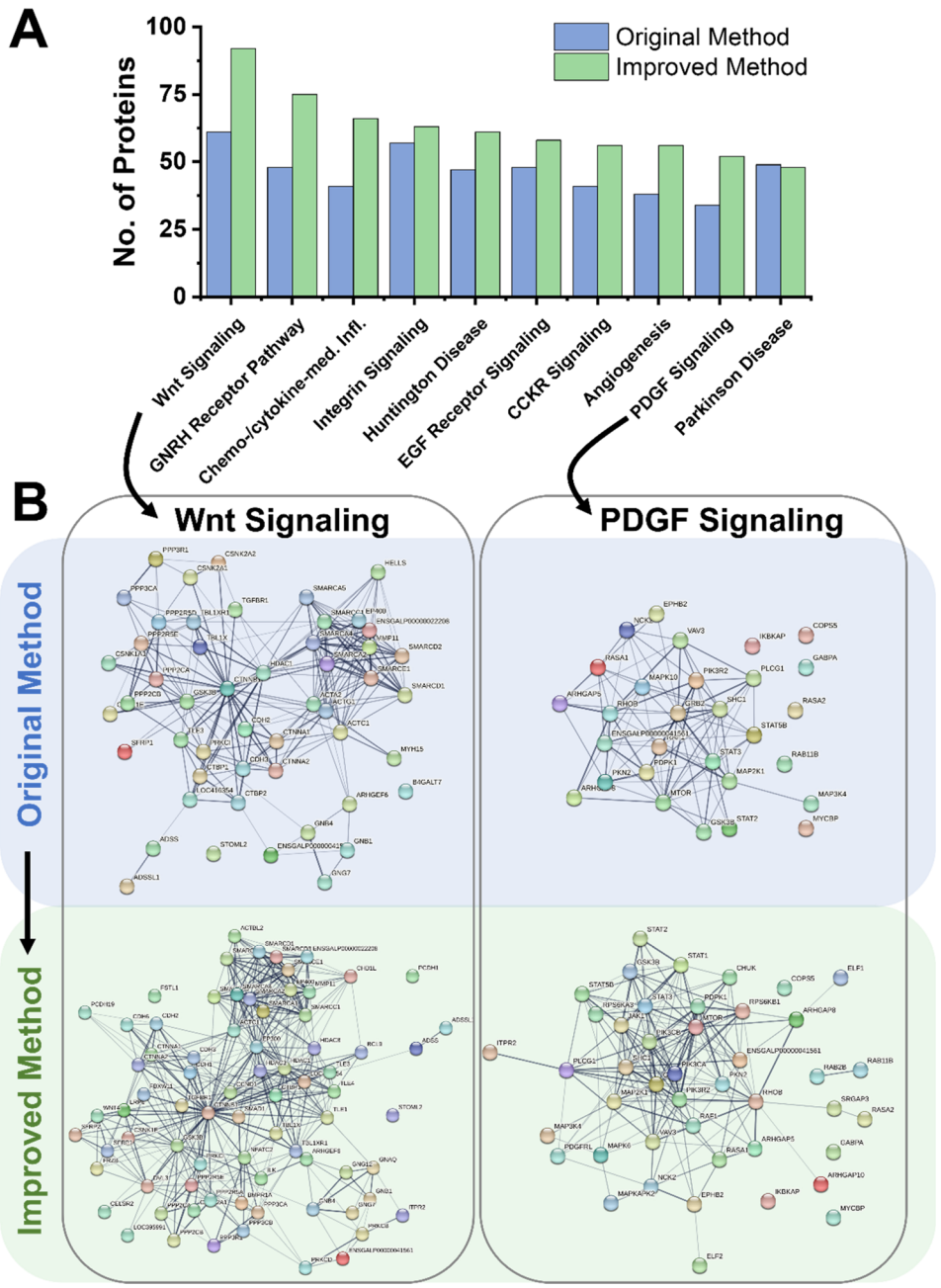

Figure 6. Biological pathways are represented by the identified proteins in the chick embryonic midbrain. (A) Comparison of the 10 statistically most significant PANTHER pathways using the original method (3680 mapped proteins, blue) and improved method (5453 mapped proteins, green). (B) STRING-predicted protein−protein interaction networks based on the identified proteins. Line thickness in the network edges indicates the strength of data support for that interaction. Abbreviations: GNRH, gonadotropin-releasing hormone; EGF, epidermal growth factor; CCKR, cholecystokinin receptor; and PDGF, platelet-derived growth factor.

confirm canonical and identify noncanonical protein players and PTMs in these processes in future studies.

Proteolysis/Extracellular Matrix Remodeling. Neural crest cell EMT requires proteolysis of cell surface proteins (e.g., cadherins and integrins) and the extracellular matrix by a disintegrin and metalloproteinase domain-containing proteins (ADAMs) and matrix metalloproteinases (MMPs) to decrease cell−cell adhesion and facilitate migration, respectively.[50] In our data set, we identified ADAM10 and MMP2, which both proteolytically cleave the detected cadherin-6B (Figure 3), leading to reduced cell−cell adhesion and delamination.[21,50] Alterations in the extracellular matrix and signals generated by its reorganization are necessary for neural crest cell migration.[51] The identified MMP2 also degrades extracellular matrix proteins such as fibronectin, laminin, vitronectin, and collagens, including collagen IV, which is highly expressed in the basement membrane of the neural tube.[52] Our data also identified transmembrane protein integrin heterodimers composed of α-5 and α-6 with β-1 subunits, which function as receptors for the detected fibronectin and laminin, promoting neural crest cell migration. Integrin binding to the identified collagen 1 α-2 leads to intracellular signaling by upregulating signals such as transforming growth factor beta (TGFβ), a known inducer of EMT.[53,54] Additionally, the

https://doi.org/10.1021/acs.jproteome.3c00291
J. Proteome Res. 2023, 22, 3264−3274

degradation of extracellular matrix associated with TGFβ promotes the availability of the latter, further inducing the TGFβ signaling pathway.[54]

Signaling Pathways. TGFβ promotes neural crest cell EMT and migration through several different signaling pathways. Binding of TGFβ to its cognate TGFβ receptor, which consists of type I and type II receptors including TGFBRI, identified in this study, leads to activation of suppressor of mothers against decapentaplegic 2 (SMAD2) and formation of a complex with SMAD3 and SMAD4 to transcriptionally regulate genes associated with EMT.[55] TGFBRI also activates protein kinase B (PKB, also known as AKT), also detected in our study, through phosphoinositide 3-kinases (PI3Ks). Interestingly, class I PI3K catalytic subunits A and B, class II subunits A and B, and regulatory subunits 2 and 4 were all identified in our analysis. This PKB activation further inhibits glycogen synthase kinase 3 alpha (GSK3) activity as well as activates the mammalian target of rapamycin complex 1 (mTORC1) and mTORC2 complexes and their pathways, promoting cell invasion and phenotypic changes associated with EMT.[56,57] Proteins comprising these complexes were also identified within this analysis and include mTOR, mitogen-activated protein kinase associated protein 1 (MAPKAP1), regulatory associated protein of mTOR complex 1 (RPTOR), and rapamycin-insensitive companion mTOR (RICTOR). Alternatively, TGFBR association with detected tumor necrosis factor receptor-associated factor 6 (TRAF6) signals further activation of mitogen-activated protein kinase kinase kinase 7 (MAP3K7, also known as TAK1), which in turn activates p38 MAPKs such as MAPK11, -13, and -14, all identified in this analysis, as well as c-Jun N-terminal kinases (JNKs) like JNK1 (also known as MAPK8) similarly identified, and these collectively impact transcription factors regulating EMT.[58]

Like TGFBR-induced signaling, signals from growth factor ligands received by associated receptor tyrosine kinases can activate the PI3K/AKT, p38 MAPK, JNK, MAPK/extracellular signal-regulated kinase (ERK), and proto-oncogene tyrosine-protein kinase sarcoma (Src) pathways. Several of these receptor tyrosine kinases were identified in this study including epidermal growth factor receptor (EGFR), fibroblast growth factor receptor 1 (FGFR1), and IGF1R, PDGFR-like protein (PDGFRL), anexelekto (AXL), discoid domain receptor family member 1 (DDR1), ephrin A2 (EPHA2), EPHB3, erythroblastic oncogene B receptor tyrosine-protein kinase B2 (ERBB2), receptor tyrosine kinase-like orphan receptor 2 (ROR2), and protein tyrosine kinase 7 (PTK7). We detected phosphorylation of IGF1R at Tyr1126, which has not been previously observed, to our knowledge. However, phosphorylation of three nearby Tyr residues is known to stabilize the kinase domain and promote phosphorylation of substrates, which may be similar for the Tyr1126 phosphorylation as well.[59] A downstream signal transduction cascade shared among many of these receptors is the rat sarcoma virus (Ras)-rapidly accelerated fibrosarcoma (Raf)-Raf-mitogen-activated protein kinase kinase (MEK)-ERK pathway. This pathway activates transcription factors that promote EMT, including Kristen RAS (KRAS), Raf1, mitogen-activated protein kinase kinase 1−6 (MAP2K1−6), and ERK1, all identified here.[60] Additionally, proteins downstream of these signaling pathways were identified as phosphorylated in our study, particularly those affected by the MAPK/ERK pathway, including Lin28b and Myc. Both of these proteins are known regulators of EMT[61] and known to be phosphorylated by the MAPK/ERK pathway. Phosphorylation of Lin28b is known to increase protein levels, which consequently promotes EMT,[62] while phosphorylation of Myc at various sites controls its stability and degradation.[63]

The canonical Wnt pathway is a well-established promoter of neural crest cell EMT, which was represented by 92 proteins in our data set (Figure 6B). Wnt ligands such as Wnt4 identified in this analysis bind to frizzled receptors and the transmembrane proteins LDL receptor-related protein (LRP) LRP5 and LRP6 detected in our analysis. This binding recruits dishevelled (DVL) proteins, like DVL2 also identified herein, and the destruction complex of CTNNB1 to the plasma membrane, leading to its inactivation.[64] In this study, we detected CTNNB1 with phosphorylation at Thr551. CTNNB1 has several reported phosphorylation sites, which have different implications such as protein degradation, stability, and translocation,[65] though Thr551 has not been identified previously. The core of this destruction complex consists of axin, GSK3, casein kinase 1, adenomatous polyposis coli (APC), and protein phosphatase 2A, and all of these proteins were identified within this study. The destruction complex binding to LRP5/6 inhibits GSK3 activity, leading to CTNNB1 accumulation in the cytoplasm and localization to the nucleus, which promotes EMT.[64] CTNND1, an enhancer of the Wnt/CTNNB1 signaling pathway that also increases EMT,[66] was identified as phosphorylated in our data set. Phosphorylation of a different serine residue on this protein is involved in the control of EMT balance.[67] On the other hand, the Wnt signaling pathway is attenuated by inhibitor proteins such as secreted frizzled related protein (sFRP) and dickkopf-related proteins, of which sFRP1 and -2 and dickkopf-related protein 3 were identified in this study.[68,69]

Transcriptional Regulation. The end results of these signaling pathways are often changes in the gene regulatory network of EMT through transcription factors or the assembly of promoter complexes. The TGFβ pathway transcriptionally regulates EMT by activating SMADs like SMAD1 and -2, both identified in this analysis, as well as the detected SMAD-interacting protein 1 (Sip1). Sip1 depletion causes neural crest cells to retain *cadherin-1* expression, negatively impacting their ability to migrate away from the neural tube.[70] TGFβ, Wnt, and Notch signaling pathways all impinge upon zinc finger protein SNAI1 (Snail1), an EMT regulator that transcribes genes important for EMT (e.g., *fibronectin*, *collagens*, *MMPs*, and *Sip1*).[54] This occurs through transcription factors and promoter complexes that enhance Snail1 transcription, including identified transcription factor nuclear factor kappa light chain enhancer of activate B cells (NF-κB), glioma-associated oncogene 2 (Gli2), and a promoter complex containing CTNNB1. Assembly of a DNA binding complex comprised of detected yes-associated protein 1 (YAP1) and transcriptional enhancer factor domain family member 1 (TEAD1) that enhances expression of EMT factors is promoted through a metabolic shift analogous to the Warburg effect in cancer cells.[71] This shift is characterized by an enrichment of rate-limiting enzymes of aerobic glycolysis such as 6-phosphofructokinase, liver type (PFKL), lactate dehydrogenase A (LDHA), and glyceraldehyde 3-phosphate dehydrogenase (GAPDH), all identified in this study.[71] Notably, YAP1 was detected as phosphorylated in our data set. YAP1 phosphorylation controls its translocation and function, as phosphorylated YAP1 is located in the cytoplasm for

https://doi.org/10.1021/acs.jproteome.3c00291
J. Proteome Res. 2023, 22, 3264−3274

degradation, where it loses its transcriptional cofactor function.[72]

CONCLUSIONS

The midbrain region of the chick embryo is home to crucial developmental processes, including EMT and migration of cranial neural crest cells, which have been previously characterized at the transcript level. In this study, we have improved nanoLC-HRMS sensitivity to enable the direct detection of >5900 proteins and >450 phosphorylated proteins, the deepest proteome coverage in the chick to date (e.g., vs 2195 protein groups from whole brain at E18[12]). Improvements in cell lysis and protein extraction and use of fractionation and a new-generation μPAC for reversed-phase separation helped to deepen the detectable proteome. The data set that is reported here also establishes the first proteomic profile of the developing chick embryo midbrain. This information in turn offers valuable insight into the developmental processes important to this tissue region, including but not restricted to key pathways related to neural crest cell EMT and migration, such as signaling, proteolysis and extracellular matrix remodeling, and transcriptional regulation. By enabling the direct quantification of thousands of proteins via HRMS, proteomics offers an accurate snapshot of the biological processes occurring in the midbrain during embryonic development, as demonstrated in this report. We anticipate that the deep proteomics method developed here can be adaptable to other regions of the brain and other developmental models. Broadened utilization of HRMS-based proteomics and enrichment methods for various PTMs in future studies will facilitate the dissection of molecular processes underlying neural crest cell EMT and migration during embryonic development.

ASSOCIATED CONTENT

Supporting Information

The Supporting Information is available free of charge at https://pubs.acs.org/doi/10.1021/acs.jproteome.3c00291.

Tables of protein identifications via standard bottom-up proteomics; protein identifications via the modified lysis protocol; protein identifications via the modified lysis protocol, 6-plexed offline fractionation, and DDA; protein identifications via the modified lysis protocol and DIA; PANTHER pathway analysis from standard vs our deep bottom-up proteomics; phosphopeptide identifications via the modified lysis protocol, 6-plexed offline fractionation, and DDA (XLSX)

AUTHOR INFORMATION

Corresponding Authors

Lisa A. Taneyhill − *Department of Animal & Avian Sciences, University of Maryland, College Park, Maryland 20742, United States*; Phone: (1) 301-405-0597; Email: ltaney@umd.edu; Fax: (1) 301-405-7980

Peter Nemes − *Department of Chemistry & Biochemistry, University of Maryland, College Park, Maryland 20742, United States*; orcid.org/0000-0002-4704-4997; Phone: (1) 301-405-0373; Email: nemes@umd.edu; Fax: (1) 301-314-9121

Authors

Kaitlyn E. Stepler − *Department of Chemistry & Biochemistry, University of Maryland, College Park, Maryland 20742, United States*; orcid.org/0000-0003-0784-089X

Seth C. Hannah − *Department of Chemistry & Biochemistry, University of Maryland, College Park, Maryland 20742, United States; Department of Animal & Avian Sciences, University of Maryland, College Park, Maryland 20742, United States*

Complete contact information is available at: https://pubs.acs.org/10.1021/acs.jproteome.3c00291

Author Contributions

K.E.S., L.A.T., and P.N. designed the experiments. S.C.H. isolated the midbrains. K.E.S. processed the samples, performed the proteomic measurements, and analyzed the data. All authors interpreted the results. All coauthors edited the manuscript.

Notes

The authors declare no competing financial interest.

ACKNOWLEDGMENTS

This work was sponsored by the National Science Foundation (award no. IOS-1947169 to L.A.T. and P.N.).

REFERENCES

(1) Simões-Costa, M.; Tan-Cabugao, J.; Antoshechkin, I.; Sauka-Spengler, T.; Bronner, M. E. Transcriptome analysis reveals novel players in the cranial neural crest gene regulatory network. *Genome Res.* **2014**, *24*, 281−290.

(2) Liu, Y. S.; Beyer, A.; Aebersold, R. On the dependency of cellular protein levels on mRNA abundance. *Cell* **2016**, *165*, 535−550.

(3) Peshkin, L.; Wuhr, M.; Pearl, E.; Haas, W.; Freeman, R. M.; Gerhart, J. C.; Klein, A. M.; Horb, M.; Gygi, S. P.; Kirschner, M. W. On the relationship of protein and mRNA dynamics in vertebrate embryonic development. *Dev. Cell* **2015**, *35*, 383−394.

(4) Shah, K.; Maghsoudlou, P. Enzyme-linked immunosorbent assay (ELISA): the basics. *Br. J. Hosp. Med.* **2016**, *77*, C98−C101.

(5) Mann, M. Can proteomics retire the Western blot? *J. Proteome Res.* **2008**, *7*, 3065−3065.

(6) Hebert, A. S.; Richards, A. L.; Bailey, D. J.; Ulbrich, A.; Coughlin, E. E.; Westphall, M. S.; Coon, J. J. The one hour yeast proteome. *Mol. Cell. Proteomics* **2014**, *13*, 339−347.

(7) Liu, D. T.; Yang, S.; Kavdia, K.; Sifford, J. M.; Wu, Z. P.; Xie, B. E.; Wang, Z.; Pagala, V. R.; Wang, H.; Yu, K. W.; et al. Deep profiling of microgram-scale proteome by Tandem Mass Tag mass spectrometry. *J. Proteome Res.* **2021**, *20*, 337−345.

(8) Aebersold, R.; Burlingame, A. L.; Bradshaw, R. A. Western blots versus selected reaction monitoring assays: time to turn the tables? *Mol. Cell. Proteomics* **2013**, *12*, 2381−2382.

(9) Mehta, D.; Ahkami, A. H.; Walley, J.; Xu, S. L.; Uhrig, R. G. The incongruity of validating quantitative proteomics using Western blots. *Nature Plants* **2022**, *8*, 1320−1321.

(10) Finnegan, S.; Robson, J. L.; Wylie, M.; Healy, A.; Stitt, A. W.; Curry, W. J. Protein expression profiling during chick retinal maturation: a proteomics-based approach. *Proteome Sci.* **2008**, *6*, 34.

(11) Bon, E.; Steegers, R.; Steegers, E. A. P.; Ursem, N.; Charif, H.; Burgers, P. C.; Luider, T. M.; Dekker, L. J. M. Proteomic analyses of the developing chicken cardiovascular system. *J. Proteome Res.* **2010**, *9*, 268−274.

(12) Uebbing, S.; Konzer, A.; Xu, L. H.; Backstrom, N.; Brunstrom, B.; Bergquist, J.; Ellegren, H. Quantitative mass spectrometry reveals partial translational regulation for dosage compensation in chicken. *Mol. Biol. Evol.* **2015**, *32*, 2716−2725.

(13) Peng, M. L.; Li, S. N.; He, Q. N.; Zhao, J. L.; Li, L. L.; Ma, H. T. Proteomics reveals changes in hepatic proteins during chicken embryonic development: an alternative model to study human obesity. *BMC Genomics* **2018**, *19*, 29.
(14) Lohraseb, I.; McCarthy, P.; Secker, G.; Marchant, C.; Wu, J.; Ali, N.; Kumar, S.; Daly, R. J.; Harvey, N. L.; Kawabe, H.; Kleifeld, O.; Wiszniak, S.; Schwarz, Q. Global ubiquitinome profiling identifies NEDD4 as a regulator of Profilin 1 and actin remodelling in neural crest cells. *Nat. Commun.* **2022**, *762*, 13.
(15) Liao, L.; Yao, Z.; Kong, J.; Zhang, X.; Li, H.; Chen, W.; Xie, Q. Transcriptomic analysis reveals the dynamic changes of transcription factors during early development of chicken embryo. *BMC Genomics* **2022**, *23*, 825.
(16) Mangum, J. E.; Farlie, P. G.; Hubbard, M. J. Proteomic profiling of facial development in chick embryos. *Proteomics* **2005**, *5*, 2542−2550.
(17) Parada, C.; Gato, A.; Aparicio, M.; Bueno, D. Proteome analysis of chick embryonic cerebrospinal fluid. *Proteomics* **2006**, *6*, 312−320.
(18) Broeckhoven, K.; Desmet, G. Advances and innovations in liquid chromatography stationary phase supports. *Anal. Chem.* **2021**, *93*, 257−272.
(19) Cong, Y. Z.; Liang, Y. R.; Motamedchaboki, K.; Huguet, R.; Truong, T.; Zhao, R.; Shen, Y. F.; Lopez-Ferrer, D.; Zhu, Y.; Kelly, R. T. Improved single-cell proteome coverage using narrow-bore packed nanoLC columns and ultrasensitive mass spectrometry. *Anal. Chem.* **2020**, *92*, 2665−2671.
(20) Hamburger, V.; Hamilton, H. L. A series of normal stages in the development of the chick embryo. 1951. *Dev. Dyn.* **1992**, *195*, 231−272.
(21) Schiffmacher, A. T.; Padmanabhan, R.; Jhingory, S.; Taneyhill, L. A. Cadherin-6B is proteolytically processed during epithelial-to-mesenchymal transitions of the cranial neural crest. *Mol. Biol. Cell* **2014**, *25*, 41−54.
(22) Demichev, V.; Messner, C. B.; Vernardis, S. I.; Lilley, K. S.; Ralser, M. DIA-NN: neural networks and interference correction enable deep proteome coverage in high throughput. *Nat. Methods* **2020**, *17*, 41−44.
(23) Gillespie, M.; Jassal, B.; Stephan, R.; Milacic, M.; Rothfels, K.; Senff-Ribeiro, A.; Griss, J.; Sevilla, C.; Matthews, L.; Gong, C. Q.; et al. The reactome pathway knowledgebase 2022. *Nucleic Acids Res.* **2022**, *50*, D687−D692.
(24) Thomas, P. D.; Ebert, D.; Muruganujan, A.; Mushayahama, T.; Albou, L. P.; Mi, H. Y. PANTHER: Making genome-scale phylogenetics accessible to all. *Protein Sci.* **2022**, *31*, 8−22.
(25) Szklarczyk, D.; Kirsch, R.; Koutrouli, M.; Nastou, K.; Mehryary, F.; Hachilif, R.; Gable, A. L.; Fang, T.; Doncheva, N. T.; Pyysalo, S.; et al. The STRING database in 2023: protein-protein association networks and functional enrichment analyses for any sequenced genome of interest. *Nucleic Acids Res.* **2023**, *51*, D638−D646.
(26) Perez-Riverol, Y.; Bai, J. W.; Bandla, C.; Garcia-Seisdedos, D.; Hewapathirana, S.; Kamatchinathan, S.; Kundu, D. J.; Prakash, A.; Frericks-Zipper, A.; Eisenacher, M.; et al. The PRIDE database resources in 2022: a hub for mass spectrometry-based proteomics evidences. *Nucleic Acids Res.* **2022**, *50*, D543−D552.
(27) Simões-Costa, M.; Bronner, M. E. Establishing neural crest identity: a gene regulatory recipe. *Development* **2015**, *142*, 242−257.
(28) Stadlmann, J.; Hudecz, O.; Krssakova, G.; Ctortecka, C.; Van Raemdonck, G.; Op De Beeck, J.; Desmet, G.; Penninger, J. M.; Jacobs, P.; Mechtler, K. Improved sensitivity in low-input proteomics using micropillar array-based chromatography. *Anal. Chem.* **2019**, *91*, 14203−14207.
(29) Sakano, H.; Zorio, D. A. R.; Wang, X. Y.; Ting, Y. S.; Noble, W. S.; MacCoss, M. J.; Rubel, E. W.; Wang, Y. Proteomic analyses of nucleus laminaris identified candidate targets of the fragile X mental retardation protein. *J. Comp. Neurol.* **2017**, *525*, 3341−3359.
(30) Meparishvili, M.; Nozadze, M.; Margvelani, G.; McCabe, B. J.; Solomonia, R. O. A proteomic study of memory after imprinting in the domestic chick. *Front. Behav. Neurosci.* **2015**, *9*, 319.
(31) Reichard, A.; Asosingh, K. Best practices for preparing a single cell suspension from solid tissues for flow cytometry. *Cytometry A* **2019**, *95A*, 219−226.
(32) Cailliez, F.; Lavery, R. Cadherin mechanics and complexation: The importance of calcium binding. *Biophys. J.* **2005**, *89*, 3895−3903.
(33) Baxi, A. B.; Lombard-Banek, C.; Moody, S. A.; Nemes, P. Proteomic characterization of the neural ectoderm fated cell clones in the Xenopus laevis embryo by high-resolution mass spectrometry. *ACS Chem. Neurosci.* **2018**, *9*, 2064−2073.
(34) Yang, F.; Shen, Y. F.; Camp, D. G.; Smith, R. D. High-pH reversed-phase chromatography with fraction concatenation for 2D proteomic analysis. *Expert Rev. Proteomics* **2012**, *9*, 129−134.
(35) Wang, H.; Sun, S. N.; Zhang, Y.; Chen, S.; Liu, P.; Liu, B. An off-line high pH reversed-phase fractionation and nano-liquid chromatography-mass spectrometry method for global proteomic profiling of cell lines. *J. Chromatogr. B* **2015**, *974*, 90−95.
(36) Wang, Y. X.; Yang, F.; Gritsenko, M. A.; Wang, Y. C.; Clauss, T.; Liu, T.; Shen, Y. F.; Monroe, M. E.; Lopez-Ferrer, D.; Reno, T.; et al. Reversed-phase chromatography with multiple fraction concatenation strategy for proteome profiling of human MCF10A cells. *Proteomics* **2011**, *11*, 2019−2026.
(37) Michalski, A.; Cox, J.; Mann, M. More than 100,000 detectable peptide species elute in single shotgun proteomics runs but the majority is inaccessible to data-dependent LC-MS/MS. *J. Proteome Res.* **2011**, *10*, 1785−1793.
(38) Tsou, C. C.; Avtonomov, D.; Larsen, B.; Tucholska, M.; Choi, H.; Gingras, A. C.; Nesvizhskii, A. I. DIA-Umpire: comprehensive computational framework for data-independent acquisition proteomics. *Nat. Methods* **2015**, *12*, 258−264.
(39) Kitata, R. B.; Yang, J. C.; Chen, Y. J. Advances in data-independent acquisition mass spectrometry towards comprehensive digital proteome landscape. *Mass Spectrom. Rev.* **2022**, e21781.
(40) Zhang, H. M.; Bensaddek, D. Narrow precursor mass range for DIA-MS enhances protein identification and quantification in *Arabidopsis*. *Life-Basel* **2021**, *11*, 982.
(41) Bruderer, R.; Bernhardt, O. M.; Gandhi, T.; Xuan, Y.; Sondermann, J.; Schmidt, M.; Gomez-Varela, D.; Reiter, L. Optimization of experimental parameters in data-independent mass spectrometry significantly increases depth and reproducibility of results. *Mol. Cell. Proteomics* **2017**, *16*, 2296−2309.
(42) Barkovits, K.; Pacharra, S.; Pfeiffer, K.; Steinbach, S.; Eisenacher, M.; Marcus, K.; Uszkoreit, J. Reproducibility, specificity and accuracy of relative quantification using spectral library-based data-independent acquisition. *Mol. Cell. Proteomics* **2020**, *19*, 181−197.
(43) Gillet, L. C.; Navarro, P.; Tate, S.; Rost, H.; Selevsek, N.; Reiter, L.; Bonner, R.; Aebersold, R. Targeted data extraction of the MS/MS spectra generated by data-independent acquisition: a new concept for consistent and accurate proteome analysis. *Mol. Cell. Proteomics* **2012**, *11*, 1−17.
(44) Searle, B. C.; Swearingen, K. E.; Barnes, C. A.; Schmidt, T.; Gessulat, S.; Kuster, B.; Wilhelm, M. Generating high quality libraries for DIA MS with empirically corrected peptide predictions. *Nat. Commun.* **2020**, *11*, 1548.
(45) Matzinger, M.; Muller, E.; Durnberger, G.; Pichler, P.; Mechtler, K. Robust and easy-to-use one-pot workflow for label-free single-cell proteomics. *Anal. Chem.* **2023**, *95*, 4435−4445.
(46) Hidalgo-Sánchez, M.; Millet, S.; Simeone, A.; Alvarado-Mallart, R. M. Comparative analysis of Otx2, Gbx2, Pax2, Fgf8 and Wnt1 gene expressions during the formation of the chick midbrain/hindbrain domain. *Mech. Dev.* **1999**, *81*, 175−178.
(47) Hollyday, M.; McMahon, J. A.; McMahon, A. P. Wnt expression patterns in chick embryo nervous system. *Mech. Dev.* **1995**, *52*, 9−25.
(48) Dady, A.; Blavet, C.; Duband, J. L. Timing and kinetics of E- to N-cadherin switch during neurulation in the avian embryo. *Dev. Dyn.* **2012**, *241*, 1333−1349.

https://doi.org/10.1021/acs.jproteome.3c00291
J. Proteome Res. 2023, 22, 3264−3274

(49) Manohar, S.; Camacho-Magallanes, A.; Echeverria, C., Jr; Rogers, C. D. Cadherin-11 Is Required for Neural Crest Specification and Survival. *Front Physiol* **2020**, *11*, 563372.
(50) Schiffmacher, A. T.; Adomako-Ankomah, A.; Xie, V.; Taneyhill, L. A. Cadherin-6B proteolytic N-terminal fragments promote chick cranial neural crest cell delamination by regulating extracellular matrix degradation. *Dev. Biol.* **2018**, *444*, S237−s251.
(51) Leonard, C. E.; Taneyhill, L. A. The road best traveled: Neural crest migration upon the extracellular matrix. *Semin. Cell. Dev. Biol.* **2020**, *100*, 177−185.
(52) Acloque, H.; Adams, M. S.; Fishwick, K.; Bronner-Fraser, M.; Nieto, M. A. Epithelial-mesenchymal transitions: the importance of changing cell state in development and disease. *J. Clin. Invest.* **2009**, *119*, 1438−1449.
(53) Maschler, S.; Wirl, G.; Spring, H.; Bredow, D. V.; Sordat, I.; Beug, H.; Reichmann, E. Tumor cell invasiveness correlates with changes in integrin expression and localization. *Oncogene* **2005**, *24*, 2032−2041.
(54) Lamouille, S.; Xu, J.; Derynck, R. Molecular mechanisms of epithelial-mesenchymal transition. *Nat. Rev. Mol. Cell Biol.* **2014**, *15*, 178−196.
(55) Xu, L.; Chen, Y. G.; Massagué, J. The nuclear import function of Smad2 is masked by SARA and unmasked by TGFbeta-dependent phosphorylation. *Nat. Cell Biol.* **2000**, *2*, 559−562.
(56) Lamouille, S.; Derynck, R. Cell size and invasion in TGF-beta-induced epithelial to mesenchymal transition is regulated by activation of the mTOR pathway. *J. Cell Biol.* **2007**, *178*, 437−451.
(57) Lamouille, S.; Connolly, E.; Smyth, J. W.; Akhurst, R. J.; Derynck, R. TGF-β-induced activation of mTOR complex 2 drives epithelial-mesenchymal transition and cell invasion. *J. Cell Sci.* **2012**, *125*, 1259−1273.
(58) Gui, T.; Sun, Y.; Shimokado, A.; Muragaki, Y. The Roles of Mitogen-Activated Protein Kinase Pathways in TGF-β-Induced Epithelial-Mesenchymal Transition. *J. Signal Transduct* **2012**, *2012*, 289243.
(59) Favelyukis, S.; Till, J. H.; Hubbard, S. R.; Miller, W. T. Structure and autoregulation of the insulin-like growth factor 1 receptor kinase. *Nat. Struct. Biol.* **2001**, *8*, 1058−1063.
(60) Gonzalez, D. M.; Medici, D. Signaling mechanisms of the epithelial-mesenchymal transition. *Sci. Signal* **2014**, *7*, re8.
(61) Liu, Y. J.; Li, H. Y.; Feng, J.; Cui, X. Y.; Huang, W.; Li, Y. D.; Su, F. X.; Liu, Q.; Zhu, J. J.; Lv, X. B.; et al. Lin28 induces epithelial-to-mesenchymal transition and stemness via downregulation of Let-7a in breast cancer cells. *PLoS One* **2013**, *8*, e83083.
(62) Tsanov, K. M.; Pearson, D. S.; Wu, Z.; Han, A.; Triboulet, R.; Seligson, M. T.; Powers, J. T.; Osborne, J. K.; Kane, S.; Gygi, S. P.; et al. LIN28 phosphorylation by MAPK/ERK couples signalling to the post-transcriptional control of pluripotency. *Nat. Cell Biol.* **2017**, *19*, 60−67.
(63) Sears, R.; Nuckolls, F.; Haura, E.; Taya, Y.; Tamai, K.; Nevins, J. R. Multiple Ras-dependent phosphorylation pathways regulate Myc protein stability. *Genes Dev.* **2000**, *14*, 2501−2514.
(64) Sutton, G.; Kelsh, R. N.; Scholpp, S. Review: The Role of Wnt/β-Catenin Signalling in Neural Crest Development in Zebrafish. *Front Cell Dev Biol.* **2021**, *9*, 782445.
(65) Shah, K. J.; Kazi, J. U. Phosphorylation-dependent regulation of WNT/Beta-catenin signaling. *Front. Oncol.* **2022**, *12*, 16.
(66) Tang, B.; Tang, F.; Wang, Z. R.; Qi, G. Y.; Liang, X. S.; Li, B.; Yuan, S. G.; Liu, J.; Yu, S. P.; He, S. Q. Overexpression of CTNND1 in hepatocellular carcinoma promotes carcinous characters through activation of Wnt/beta-catenin signaling. *J. Exp. Clin. Cancer Res.* **2016**, *35*, No. 82, DOI: 10.1186/s13046-016-0344-9.
(67) Yang, J.; Bassuk, A. G.; Merl-Pham, J.; Hsu, C. W.; Colgan, D. F.; Li, X. R.; Au, K. S.; Zhang, L. J.; Smemo, S.; Justus, S.; et al. Catenin delta-1 (CTNND1) phosphorylation controls the mesenchymal to epithelial transition in astrocytic tumors. *Hum. Mol. Genet.* **2016**, *25*, 4201−4210.
(68) Leyns, L.; Bouwmeester, T.; Kim, S. H.; Piccolo, S.; De Robertis, E. M. Frzb-1 is a secreted antagonist of Wnt signaling expressed in the Spemann organizer. *Cell* **1997**, *88*, 747−756.
(69) Bafico, A.; Liu, G.; Yaniv, A.; Gazit, A.; Aaronson, S. A. Novel mechanism of Wnt signalling inhibition mediated by Dickkopf-1 interaction with LRP6/Arrow. *Nat. Cell Biol.* **2001**, *3*, 683−686.
(70) Rogers, C. D.; Saxena, A.; Bronner, M. E. Sip1 mediates an E-cadherin-to-N-cadherin switch during cranial neural crest EMT. *J. Cell Biol.* **2013**, *203*, 835−847.
(71) Bhattacharya, D.; Azambuja, A. P.; Simoes-Costa, M. Metabolic reprogramming promotes neural crest migration via YAP/TEAD signaling. *Dev. Cell* **2020**, *53*, 199−211.
(72) Cheng, D.; Jin, L.; Chen, Y. H.; Xi, X. Y.; Guo, Y. YAP promotes epithelial mesenchymal transition by upregulating Slug expression in human colorectal cancer cells. *Int. J. Clin. Exp. Pathol.* **2020**, *13*, 701−710.

https://doi.org/10.1021/acs.jproteome.3c00291
J. Proteome Res. 2023, 22, 3264−3274